Proceedings of the ASME 2024 43rd International Conference on Ocean, Offshore and Arctic Engineering
OMAE2024
June 9-14, 2024, Singapore, Singapore

OMAE2024-126583

SERVICE LIFE PREDICTION METHOD FOR A FREE SPANNING PIPELINE UNDERGOING VORTEX INDUCED VIBRATIONS

Qing-Yuan Song
[1.] Institute of Mechanics, Chinese Academy of Sciences, Beijing100190, China
[2.] School of Engineering Science, University of Chinese Academy of Sciences, Beijing 100049, China
Email: songqingyuan@imech.ac.cn

Jun Liu
[1.] Institute of Mechanics, Chinese Academy of Sciences, Beijing100190, China
[2.] School of Engineering Science, University of Chinese Academy of Sciences, Beijing 100049, China
Email: liujun@imech.ac.cn

Fu-Ping Gao*
[1.] Institute of Mechanics, Chinese Academy of Sciences, Beijing100190, China
[2.] School of Engineering Science, University of Chinese Academy of Sciences, Beijing 100049, China
Email: fpgao@imech.ac.cn
(Corresponding Author)

ABSTRACT

Free spans of a subsea pipeline may undergo vortex-induced vibrations (VIVs) and could be damaged by fatigue failure. The free span length is a key parameter for determining the structural natural frequency, which would correspondingly influence the reduced velocity (*Vr*) for the VIV responses. The existing flume tests indicated that the VIVs of a near-bed cylinder may be triggered effectively in moderate shear flows. This may imply that the vibration cycles of a free spanning pipeline could be up to ten-millions, and the very-high-cycle fatigue (VHCF) could be encountered during the engineering service. On the basis of the dimensionless vibration amplitude *A/D-Vr* curve and the recommended S-N curve for the high-strength steel pipelines with cathodic protection under seawater environments, a prediction method is proposed for the service life of a free spanning pipeline undergoing VIVs. A case study is then performed to evaluate the service life (in terms of vibration cycles) of the free-spans with the focus on VHCF. It is indicated that, if the characteristic flow velocity is given, the variation of the service life with the span length is generally nonlinear, which is attributed to being involved in various VIV branches of the *A/D-Vr* curve.

Keywords: Free spanning pipeline; Vortex-induced vibration; Service life prediction; Very-high-cycle fatigue; Pipeline-seabed interaction

NOMENCLATURE

A	Vibration amplitude of the cylinder
$\bar{a}$	Coefficient in Eq. (8)
C_1	Boundary condition coefficient in Eq. (2)
C_3	Boundary condition coefficient in Eq. (2)
C_A	Added mass coefficient
D	Outer diameter of the cylinder
D_o	Outer diameter of the pipe
D_i	Inner diameter of the pipe
e	Gap between the pipe bottom and the seabed surface
E	Elastic modulus of the pipe
F_{CS}	Concrete stiffness enhancement factor for the pipe
f_n	Natural frequency of the pipe or cylinder
f_v	Frequency of vortex-shedding from a fixed cylinder
I	Moment of inertia
K_s	Combined mass-damping parameter
k	Exponent on thickness of the pipe
L	Free span length of the pipeline
L_{eff}	Effective span length
M	Bending moment of the pipe
m_a	Added mass of the pipeline per meter
m_c	Mass of the content inside the pipeline per meter
m_e	Effective mass of the pipeline per meter
m_p	Mass of the steel pipeline per meter
N	Number of cycles to failure
P_{cr}	Critical buckling load
q	Uniform load on the pipeline

SCF	Stress concentration factor
S_{eff}	Effective axial force along the pipeline
t	Wall thickness of the pipe
t_{ref}	Reference wall thickness of the pipe
U	Flow velocity
Vr	Reduced velocity
Vr_{cr}	Critical reduced velocity
w	Deflection of the suspended pipeline
w_{max}	Maximum deflection of the suspended pipeline
β	Relative soil stiffness parameter
δ	Static deflection of the pipeline
$\Delta\sigma$	Stress range
ρ_{steel}	Density of the steel
ρ_{water}	Density of the seawater
σ	Normal stress
σ_{max}	Maximum normal stress
υ_{water}	Kinematic viscosity of the seawater

1. INTRODUCTION

Subsea pipelines have been widely employed for transporting oil and gas from underwater wells to offshore platforms and onshore processing facilities. The pipeline free-span scenario could be permanent when generated by seabed unevenness or by artificial supports for pipeline crossing, or be generated with short- to long-term evolution by seabed mobility and local scour in shallow waters (Drago *et al.*, 2015). Under the action of ocean currents, a partially-embedded pipeline may also be suspended because of the tunnel-erosion (Sumer *et al.*, 1988; Gao, 2017; Shi *et al.*, 2021). As such, the free-spans could be frequently encountered or even inevitable, especially for a long-laid pipeline in the oil and gas exploitation in deep waters.

In the harsh subsea environments, a pipeline free-span may suffer from vortex-induced vibrations (VIVs), as illustrated in Fig. 1. For an elastically-mounted cylinder, the transverse VIVs can be effectively triggered when the reduced velocity (Vr) approaches a critical value $Vr_{\text{cr}} \approx 4.0$ under wall-free conditions (Blevins, 1990). The reduced velocity Vr is defined as:

$$Vr = \frac{U}{f_{\text{n}} D} \tag{1}$$

where U is the characteristic velocity of the flow perpendicular to the cylinder's axis, f_{n} is the structural natural frequency, and D is the outer diameter of the cylinder. Once the VIVs are initiated, the frequency of vortex-shedding and that of the structural oscillation would collapse into an identical value, which is known as "lock-in" or "synchronization" phenomenon. The maximum amplitude of the vibration principally depends on the combined mass-damping parameter K_{s} (Williamson and Govardhan, 2004). In the engineering practices, subsea pipelines are usually in the proximity to the seabed. For such a near-bed cylinder, the flow fields around the cylinder would be altered due to bed-proximity effects, which would affect the VIVs responses subsequently. Recently, Liu and Gao (2022) investigated the bed-proximity effects on triggering transverse vibration of a cylinder under low K_{s} conditions. It was found that, as the cylinder getting closer to the bed boundary (i.e., with the decrease of the gap-to-diameter ratio e/D from 2.0 to 0.1), the values of Vr_{cr} significantly decrease (from 4.0 to 2.85), which is accompanied by the decrease of vibration amplitudes. Previous flume observations by Gao *et al.* (2006) indicated that, once the VIVs are triggered, the local scour around the vibrating pipe would be greatly enhanced due to the cyclic vibrations, e.g., the scour depth could be up to approximately 1.2D, which can be regarded as the wall-free condition for VIV responses.

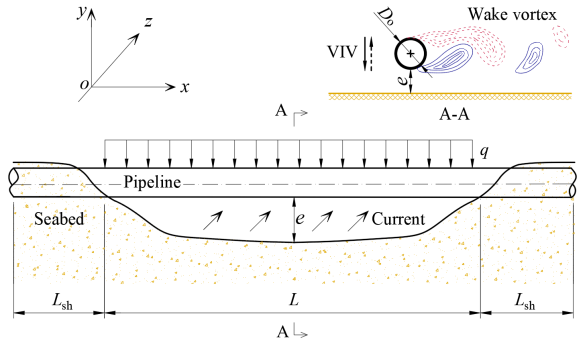

Figure 1. Schematic diagram of a pipeline free-span undergoing VIVs (not in scale).

In the engineering practice, fatigue may take place under the cyclic loading after a substantial period of service. The fatigue limit stress is generally defined as the highest stress at which the specimen do not fail after 10^7 loading cycles. However, the existing studies have extended knowledge by warning that fatigue failure may occur at lifetime greater than $N = 10^7$ at a stress that is lower than the conventional fatigue limit (Sharma *et al.*, 2020). Generally speaking, fatigue of metallic materials can be divided into three regions: low cycle fatigue (LCF), high cycle fatigue (HCF) and very high cycle fatigue (VHCF) in which the number of cycles to failure is beyond 10^7. The fatigue behavior in the VHCF region is quite different compared to that in the conventional HCF (Murakami *et al.*, 2000; Shiozawa *et al.*, 2001; Sakai *et al.*, 2002; Hong *et al.*, 2012; Song and Sun, 2020). For instance, the fatigue behaviors of high-strength steels in the VHCF region show crack initiation at the inclusion site, while in HCF region, the cracks are located preferentially at the surface (Sharma *et al.*, 2020). The influence of hydrogen was found to be crucial for eliminating the fatigue limit in the extremely high cycle fatigue (Murakami *et al.*, 2000; Sharma *et al.*, 2020).

For offshore structures subjected to typical wave and wind loading, significant fatigue damage may occur for $N \geqslant 10^7$ cycles, i.e., in the VHCF region (DNVGL, 2016). It is also very

common that turbine blades experience stress cycles more than $N=10^7$ by vibration. Nevertheless, fatigue test data are normally derived for number of cycles less than 10^7, including those for subsea pipeline steels. For the scenario of free-spanning pipelines, the fatigue by VIVs is of great concern in the engineering design (DNVGL, 2017). The allowable span length of a suspended pipeline was investigated by considering VIV hysteresis effects (Liu and Gao, 2021). The natural frequency of free-spans was assessed by using finite element model (He *et al.*, 2020), and the random ocean current induced fatigue life of free-spans was further predicted on the basis of the Palmgren-Miner cumulative damage rule. Nevertheless, the correlation between the free-span length and the corresponding service life has not been well revealed, especially in the VHCF region.

In this investigation, a service life prediction method is proposed for the free-spanning pipeline undergoing VIVs. Based on the existing test results on transverse VIV response, the *A/D*-*Vr* curve with four branches is created (note: *A/D* is the ratio of the VIV amplitude to the pipe diameter). The bilinear S-N (Stress range - Number of cycles to failure) curves are recommended by considering the VHCF of the high-strength steel pipelines with cathodic protection under seawater environments. A flow chart is provided for the service life prediction of a free-spanning pipeline undergoing VIVs. A case study is then performed to evaluate the service life of the pipeline free-span with the focus on VHCF. The correlations between the service life and the flow velocity or the free-span length are finally established.

2. VIBRATION AMPLITUDE AND STRESS DISTRIBUTION ALONG THE FREE-SPANNING PIPELINE

2.1 Amplitude of VIVs

The natural frequency of a free-span or suspended pipeline is a key factor in identifying the reduced velocity (see Eq. (1)). The natural frequency or the first eigen frequency of a free-spanning pipeline is influenced by many factors (such as span length, elastic modulus of the pipe steel, boundary conditions, effective mass, and moment of inertia of the pipe, etc.), which can be evaluated with the following equation:

$$f_n \approx \frac{C_1}{L_{eff}^2}\left(\frac{(1+F_{CS})EI}{m_e}\left[1+\frac{S_{eff}}{P_{cr}}+C_3\left(\frac{\delta}{D}\right)^2\right]\right)^{\frac{1}{2}} \quad (2a)$$

where L_{eff} is the effective span length; m_e is the effective mass of the pipeline; F_{CS} is the concrete stiffness enhancement factor; E is the modulus of elasticity of the steel pipeline; I is the inertia moment of the steel pipeline; S_{eff} is the effective axial force (negative in compression); P_{cr} is the critical buckling load (positive sign); δ is the static deflection; C_1 and C_3 are the end boundary condition coefficients, which depend on the support conditions of the free-span boundary (DNVGL, 2017). The effective span length L_{eff} can be determined by

$$\frac{L_{eff}}{L}=\begin{cases}\dfrac{4.73}{-0.066\beta^2+1.02\beta+0.63} & \beta \geq 2.7\\ \dfrac{4.73}{0.036\beta^2+0.61\beta+1.0} & \beta < 2.7\end{cases} \quad (2b)$$

in which, β is the relative soil stiffness parameter. The basic rules for the ideal end conditions are as follows (DNVGL, 2017; Guo *et al.*, 2014):

(1) Pinned-Pinned: used for free-spans where each end is allowed to rotate about the pipeline axis;
(2) Fixed-Fixed: should be used for the free-spans that are fixed in place by some sort of anchor at both ends.

The following values of C_1 in Eq. (2a) have been widely used for these typical end conditions: (1) $C_1 = 1.57$ for the Pinned-Pinned end condition; (2) $C_1 = 3.56$ for the Fixed-Fixed end condition. The effective mass per meter (m_e) is the sum of mass of the steel pipe per meter (m_p), the mass of the content inside the pipe per meter (m_c) and the added mass per meter (m_a):

$$m_e = m_p + m_c + m_a \quad (3a)$$

$$m_a = C_A\frac{\pi\rho_{water}D^2}{4} \quad (3b)$$

where C_A is the added mass coefficient (for a circular pipeline, $C_A = 1.0$); and ρ_{water} is the density of the seawater.

If the effective axial force and the static deflection are not taken into account, Eq. (2a) can then be simplified as:

$$f_n \approx \frac{C_1}{L_{eff}^2}\left(\frac{(1+F_{CS})EI}{m_e}\right)^{\frac{1}{2}} \quad (4)$$

In the past few decades, the VIVs of an elastically-mounted cylinder have been investigated by quite a few researchers, see the comprehensive reviews, e.g., Williamson and Govardhan (2004), Sarpkaya (2004), Bearman (2011) and Wu *et al.* (2012). In this study, the VIV amplitudes of wall-free cylinders in the region of low mass-damping parameter K_s (broadly $K_s < 0.05$, see Williamson and Govardhan, 2004) are collected from some benchmark flume observations. The whole curve for the nonlinear variation of *A/D* with *Vr* is created as shown in Fig. 2. As indicated in Fig. 2, in such a low mass-damping system, four distinct stages of VIV responses can be identified, namely the "initial excitation branch", the "upper branch", the "lower branch" and the "desynchronization" (also see Khalak and Williamson, 1997). In the "initial excitation branch" (i.e. $Vr < 4.5$), the cylinder starts to vibrate with a relatively small amplitude; in the "upper branch" ($4.5 \leq Vr < 7.0$), the cylinder vibrates with large amplitude; in the "lower branch"

($7.0 \le Vr < 12$), the cylinder vibrates with a moderate amplitude; and in the "desynchronization" ($Vr \ge 12$), the vibration amplitude of a wall-free circular cylinder is further reduced.

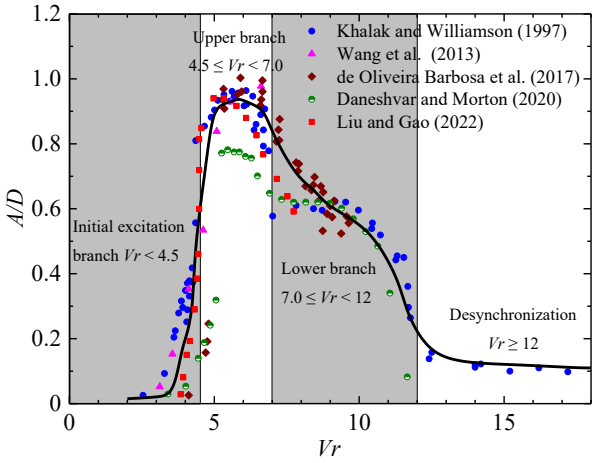

Figure 2. *A/D-Vr* curve for a wall-free circular cylinder with low mass-damping parameter.

Above analyses indicate that once the pipeline parameters and the flow velocity (U) are given, the corresponding reduced velocity (Vr) can be calculated with Eq. (1) and Eq. (4), and the vibration amplitude can be obtained with the reference to Fig. 2.

2.2 Stress distribution along the free span

It is supposed that the ocean current is perpendicular to the axis of the free spans, as illustrated in Fig. 1. As stated above, the shoulders for a free-span can be simplified as the Pinned-Pinned or the Fixed-Fixed end condition. The maximum deflection in the middle of the span (w_{max}) under the action of a uniform load (q) can be calculated with Eq. (5a) for the Pinned-Pinned end condition, and with Eq. (5b) for the Fixed-Fixed end condition, respectively:

$$w_{max} = \frac{5qL^4}{384EI} \tag{5a}$$

$$w_{max} = \frac{qL^4}{384EI} \tag{5b}$$

where L is the span length. Similarly, the maximum bending moment correlated with the maximum deflection in the middle of the free span can be calculated with Eq. (6a) for the Pinned-Pinned end condition, and with Eq. (6b) for the Fixed-Fixed end condition, respectively:

$$M_{max} = \frac{48EI}{5L^2} w_{max} \tag{6a}$$

$$M_{max} = \frac{32EI}{L^2} w_{max} \tag{6b}$$

Fig. 3 (a) and (b) show the distributions of bending moment along the free-span under these two end conditions. It is indicated that the bending moment reaches its peak value in the middle of the span under the Pinned-Pinned end condition. But under the Fixed-Fixed end condition, the two ends connected with the span shoulders undertake the maximum bending moment.

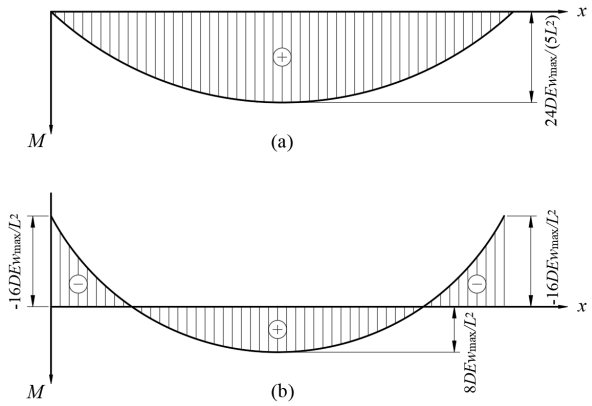

Figure 3. Distributions of bending moment along the free-span: (a) under the Pinned-Pinned end condition; (b) under the Fixed-Fixed end condition.

Consequently, the maximum normal stresses (σ_{max}) correlated with maximum deflections (w_{max}) can be expressed as

$$\sigma_{max} = \frac{24DE}{5L^2} w_{max} \tag{7a}$$

$$\sigma_{max} = \frac{16DE}{L^2} w_{max} \tag{7a}$$

for the Pinned-Pinned and the Fixed-Fixed end condition, respectively.

3. RECOMMENDED S-N CURVES

The fatigue design is generally based on use of S-N curves, which were obtained from fatigue tests. The number of cycles to failure (N) at a stress range ($\Delta\sigma$) is defined by an S-N curve. As aforementioned, significant fatigue damage to offshore structures usually occurs for $N \ge 10^7$ cycles (VHCF region). On the VHCF mechanism of metallic materials, a few studies have already been carried out, e.g., Murakami *et al.* (2000), Shiozawa *et al.* (2001), Sakai *et al.* (2015), and Hong *et al.* (2016). It has been generally recognized that the cracks usually initiate from the surface of materials in LCF and HCF regions, while the cracks preferably emerge in the interior of the materials with fish-eye morphology in VHCF region. As illustrated in Fig.

4, an inclusion was found at the center of the fish-eye zone. The rough area surrounding the inclusion within the fish-eye zone, named fine granular area (FGA), is the crack initiation region, which is critical to the VHCF occurrence. The initiation and early growth of cracks could be attributed to the grain refinement caused by the dislocation interaction over a number of cyclic loads followed by the formation of micro-cracks; but the micro-cracks could also be formed, irrespective of the grain refinement during the cyclic loading (Song and Sun, 2020).

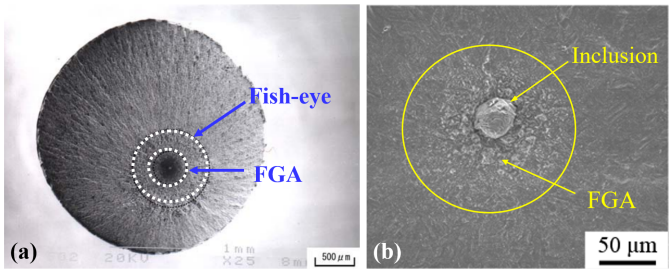

Figure 4. (a) The fracture surface of a high strength steel (Sakai, 2009) (b) A close-up for the crack initiation region of a high strength steel (Song, 2021).

For the sake of service safety, an unfavorable scenario is considered in this case study, e.g., the weld joint is happened to be installed in the middle of the span for the Pinned-Pinned boundary condition and in one end of the span for the Fixed-Fixed boundary condition. The service environment is considered to be in the seawater and with cathodic protection (CP).

The fatigue test data are normally derived for number of cycles less than 10^7. As such, how to extrapolate the fatigue test data into the VHCF region is important in order to achieve a reliable assessment procedure (DNVGL, 2016). The bilinear S-N curves, i.e., F3 and C1 (see Fig. 5), are recommended to define the number of cycles to failure at stress range $\Delta\sigma$. Note that, the F3 curve is for the circumferential butt weld made from one side without a backing bar; and the C1 curve is for the circumferential butt welds made from one side that are machined or ground flush to remove defects and weld overfill (see DNVGL, 2016). Meanwhile, the existing fatigue test data for the high strength steels under various environments are also provided in Fig. 5 for references. The structural stress concentration factor SCF = 1.61 for the S-N curve F3, and SCF = 1.0 for the S-N curve C1. As shown in Fig. 5, the S-N curves in VHCF region get more horizontal as the number of cycles to failure N becomes larger than 10^6. The recommended S-N curves can be expressed in the form:

$$\mathrm{Log}_{10}(N) = \mathrm{Log}_{10}(\bar{a}) - m\mathrm{Log}_{10}\left(\Delta\sigma\left(\frac{t}{t_{\mathrm{ref}}}\right)^{k}\right) \qquad (8)$$

where m is the negative inverse slope of the S-N curve, $\mathrm{Log}_{10}(\bar{a})$ is the intercept of $\mathrm{Log}_{10}(N)$ axis, t_{ref} is the reference wall thickness of the pipe for welded connections, and k is the thickness exponent on fatigue strength.

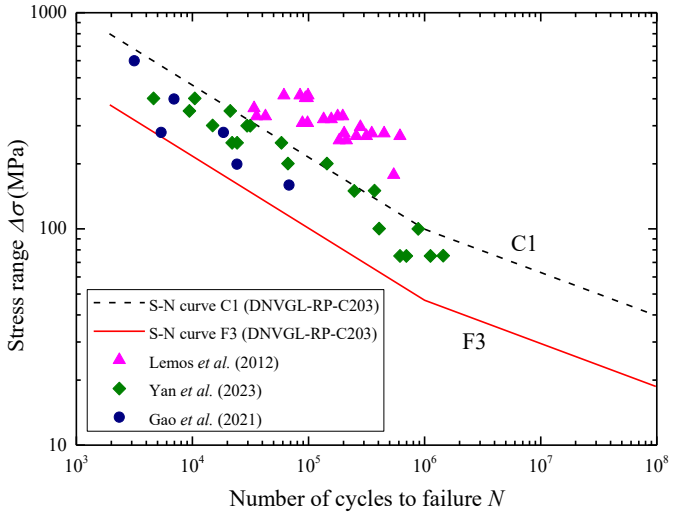

Figure 5. Recommended S-N curves for the high strength steel pipelines in the seawater and with cathodic protection (adapted from DNVGL (2016)), and the existing test data by Lemos *et al.* (2012) for the saline environments saturated with carbon dioxide; Yan *et al.* (2023) for the saturated H_2S solution; Gao *et al.* (2021) for NACE solution with saturated H_2S.

4. FATIGUE LIFE PREDICTION AND DISCUSSIONS

4.1 A flow chart for service life prediction

A flow chart is proposed for the service life prediction of a free-spanning pipeline undergoing VIVs, as illustrated in Fig. 6. A brief description of the analysis procedure is given as follows:

(1) For given structural parameters, the natural frequency (f_n) of the free-span is firstly calculated with Eqs. (3a), (2b) and (2a), which is a crucial factor for calculating the reduced velocity (Vr).

(2) Once the value of Vr is obtained, the vibration amplitude (A/D) can then be evaluated with the reference to the recommended A/D-Vr curve (Fig. 2). Subsequently, the maximum stress range ($\Delta\sigma$) can be calculated with Eq. (7).

(3) By referring to the recommended S-N curves (Fig. 5), the service life of the free-spanning pipeline can be finally obtained.

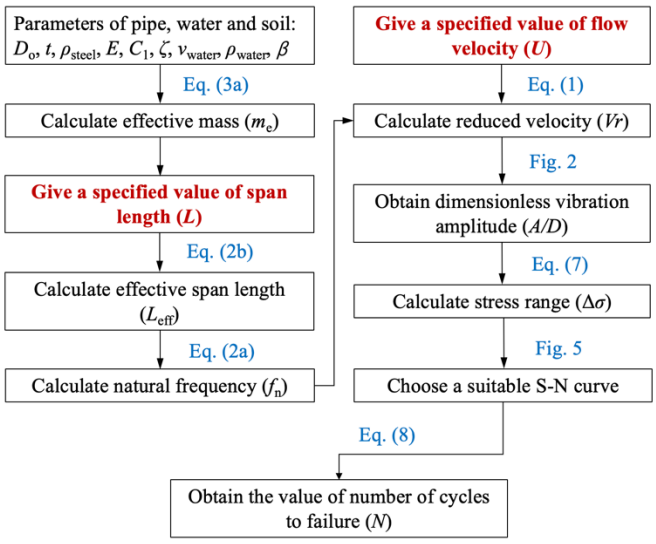

Figure 6. Flow chart for the service life prediction of a free-spanning pipeline undergoing VIVs.

4.2 Case study and discussions

A subsea pipeline with the outer diameter of 20 inches (0.508 m) is considered for a case study. The parameters of the steel pipe, the gas inside the pipe and seawater are shown in Table 1. The values of the key parameters for the S-N curves are listed in Table 2. For the extreme scenario of large free-spans, the values of span length are examined in the range from 60 m to 130 m. The free-span under the Fixed-Fixed end condition is considered in the case study. Note that, the end condition of the free-span has a significant influence on the natural frequency (f_n) of the free-spanning pipeline, which would further alter the values of Vr (see Eq. (1)). As the variation of A/D with Vr is nonlinear (see Fig. 2), the correlations between the service life and the flow velocity or span length can be obtained by following the flow chart as shown in Fig. 6.

Table 1. Parameters for a case study

Parameters	Values	Units
Outer diameter of the steel pipe (D_o)	0.508	m
Wall thickness of the steel pipe (t)	0.0379	m
Density of the steel (ρ_{steel})	7.870×10^3	kg/m^3
Density of the gas inside the pipe (ρ_{cont})	0.200×10^3	kg/m^3
Density of the seawater (ρ_{water})	1.024×10^3	kg/m^3
Kinematic viscosity of seawater (υ_{water})	1.565×10^{-6}	m^2/s
Elastic modulus of the steel (E)	2.10×10^{11}	Pa
Moment of inertia for the steel pipe (I)	1.56×10^{-3}	m^4
Relative soil stiffness (β)	4.0	
Reference wall thickness of the pipe (t_{ref})	0.025	m

Table 2. Parameters for the S-N curve

S-N curve	$N\leq10^6$		$N>10^6$		k
	m_1	$\mathrm{Log}_{10}(\bar{a}_1)$	m_2	$\mathrm{Log}_{10}(\bar{a}_2)$	
C1	3	12.049	5	16.081	0.10
F3	3	11.146	5	14.576	0.25

For a given span length L = 90 m, the variations of fatigue life with flow velocity are shown in Fig. 7. In the "initial branch", i.e. $U < 0.41$ m/s ($Vr < 4.5$), the free-span starts to vibrate. With the increase of the flow velocity, the fatigue life decreases. In the "upper branch", i.e. $0.41 \leq U < 0.65$ m/s ($4.5 \leq Vr < 7.0$), the free-span vibrates with large amplitudes, so that the fatigue life is reduced. In the "lower branch", i.e. $0.65 \leq U < 1.10$ m/s ($7.0 \leq Vr < 12$), the free-span vibrates with moderate amplitudes, and the corresponding fatigue life becomes longer. Similarly, in the "desynchronization", i.e. $U \geq 1.10$ m/s ($Vr \geq 12$), the free span vibrates with smaller amplitudes and the fatigue life becomes longer.

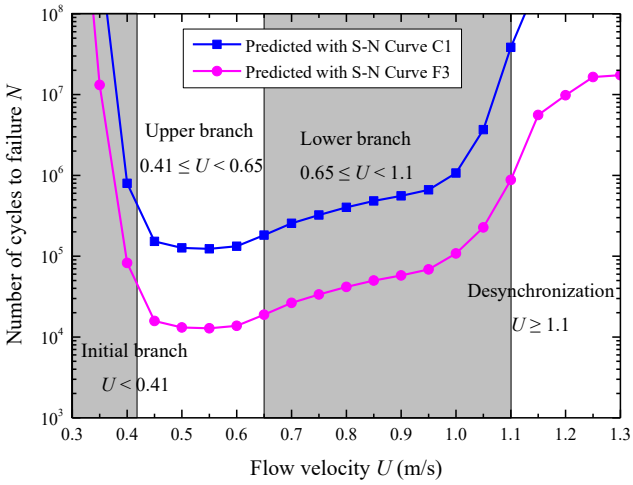

Figure 7. Variations of number of cycles to failure (N) with flow velocity (U) for the typical value of span length (L = 90 m).

For a given flow velocity U = 0.57 m/s, the variations of fatigue life with span length (L) are shown in Fig. 8. For $L < 77$ m, the free-span starts to vibrate with the increase of the span length, i.e. the "initial branch". When the span length $77 \leq L < 96$ m, the free span vibrates with a very large amplitude, i.e. the "upper branch", so the fatigue life is very short. For $96 \leq L < 125$ m, the vibration amplitude becomes smaller, i.e. the "lower branch", therefore the fatigue life becomes longer. For $L \geq 125$ m, the vibration amplitude continues to decrease, i.e. the "desynchronization", the fatigue life becomes larger.

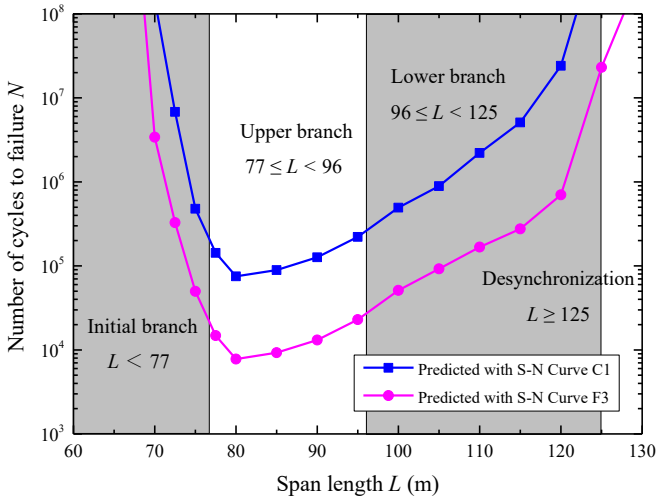

Figure 8. Variations of number of cycles to failure (N) with span length (L) for the typical value of flow velocity (U = 0.57 m/s).

From the analysis above, it may be found that the relationships between the fatigue life (in terms of number of cycles to failure N) and the flow velocity (U) or the span length (L) are generally nonlinear, which is attributed to the nonlinear variation of the reduced velocity (Vr) with the dimensionless vibration amplitude (A/D). As shown in Figs. (7)-(8), when the flow velocity (U) or the span length (L) is relatively small, i.e., the vibration falls into the initial branch with small amplitudes the pipeline could be damaged by very-high-cycle fatigue (VHCF). This situation happens to be the VIVs of a near-bed cylinder, which could be triggered effectively with small vibration amplitudes in a moderate shear flow (see Liu and Gao, 2021; 2022).

5. CONCLUDING REMARKS

(1) In this study, with the reference to the benchmark flume observations on VIV response amplitudes of a low mass-damping system, the whole curve for the nonlinear variation of A/D with Vr (i.e. the A/D-Vr curve) is recommended, in which four distinct stages of VIV response can be identified, i.e. the "initial excitation branch", the "upper branch", the "lower branch" and the "desynchronization". Bilinear S-N curves were chosen to describe the relation between the stress range and the service life of free-spanning pipelines under the complex seawater environment.

(2) On the basis of the recommended A/D-Vr curve and the S-N curve for the very-high-cycle fatigue of a high-strength steel in the seawater and with cathodic protections, a prediction method is proposed for the service life of free-spanning pipelines undergoing VIVs. If the pipeline and environmental parameters are given, the service life in terms of number of cycles to failure N can be evaluated following the flow chart.

(3) The results of a case study indicate that the variations of the fatigue life with the flow velocity or the free-span length are generally nonlinear, which is attributed to being involved in various VIV branches in the A/D-Vr curve.

ACKNOWLEDGMENTS

This work is financially supported by the National Natural Science Foundation of China (Grant Nos. 11825205 and 12061160463).

REFERENCES

[1] Bearman P.W., 2011, "Circular cylinder wakes and vortex-induced vibrations", *Journal of Fluids and Structures,* Vol. 27, 648-658.

[2] Blevins R.D., 1990, "Flow-Induced Vibration," 2nd ed, New York: Krieger Publishing Company.

[3] Det Norske Veritas and Germanischer Lloyd (DNVGL), 2016, "*DNVGL-RP-C203: Fatigue Design of Offshore Steel Structures*".

[4] Det Norske Veritas and Germanischer Lloyd (DNVGL), 2017, "*DNVGL-RP-F105: Free Spanning Pipelines*".

[5] Drago M., Mattioli M., Bruschi R., et al., 2015, "Insights on the design of free spanning pipelines", *Philosophical Transactions of the Royal Society A,* Vol. 373, 20140111.

[6] Gao F.P., 2017, "Flow-pipe-soil coupling mechanisms and predictions for submarine pipeline instability", *Journal of Hydrodynamics, Series B,* Vol. 29(5), 763-773.

[7] Gao F.P., Yang B., Wu Y. X., Yan S.M., 2006, "Steady currents induced seabed scour around a vibrating pipeline", *Applied Ocean Research*, Vol. 28(5): 291-298.

[8] Gao Z., Gong B., Xu Q., et al., 2021, "High cycle fatigue behaviors of API X65 pipeline steel welded joints in air and H_2S solution environment", *International Journal of Hydrogen Energy,* Vol. 46(17), 10423-10437.

[9] Guo B, Song S, Ghalambor A, et al., 2014, "Offshore Pipelines: Design, Installation, and Maintenance", 2nd ed, Waltham: Gulf Professional Publishing.

[10] He Z.F., Wei Y., Liu S.L., 2020, "Analysis of safe span length and fatigue life of submarine pipelines", *China Ocean Engineering*, Vol. 34(1), 119-130.

[11] Hong Y., Liu X., Lei Z., et al., 2016, "The formation mechanism of characteristic region at crack initiation for very-high-cycle fatigue of high-strength steels", *International Journal of Fatigue*, Vol. 89, 108-118.

[12] Hong Y., Zhao A., Qian G., et al., 2012, "Fatigue strength and crack initiation mechanism of very-high-cycle fatigue for low alloy steels", *Metallurgical and Materials Transactions A*, Vol. 43, 2753-2762.

[13] Khalak A., Williamson C.H.K., 1997, “Investigation of the relative effects of mass and damping in vortex-induced vibration of a circular cylinder”, *Journal of Wind Engineering and Industrial Aerodynamics*, Vol. 69-71, 341-350.

[14] Lemos M., Kwietniewski C., Clarke T., et al., 2012, “Evaluation of the fatigue life of high-strength low-alloy steel girth welds in aqueous saline environments with varying carbon dioxide partial pressures”, *Journal of Materials Engineering and Performance,* Vol. 21(7), 1254-1259.

[15] Liu J., Gao F.P., 2021, “Evaluation for allowable span length of a submarine pipeline considering VIV hysteresis effect”, *International Journal of Offshore and Polar Engineering*, Vol. 31(3), 325-332.

[16] Liu J., Gao F.P., 2022, “Triggering mechanics for transverse vibrations of a circular cylinder in a shear flow: Wall-proximity effects”, *Journal of Fluids and Structures,* Vol. 108, 103423.

[17] Murakami Y., Nomoto T., Ueda T., et al., 2000, “On the mechanism of fatigue failure in the superlong life regime ($N>10^7$ cycles). Part I: influence of hydrogen trapped by inclusions”, *Fatigue & Fracture of Engineering Materials & Structures*, Vol. 23, 893-902.

[18] Sakai T., 2009, “Review and prospects for current studies on very high cycle fatigue of metallic materials for machine structural use”, *Journal of Solid Mechanics and Materials Engineering,* Vol. 3, 425-439.

[19] Sakai T., Oguma N., Morikawa A., 2015, “Microscopic and nanoscopic observations of metallurgical structures around inclusions at interior crack initiation site for a bearing steel in very high-cycle fatigue”, *Fatigue and Fracture of Engineering Materials and Structures,* Vol. 38, 1305-1314.

[20] Sakai T., Sato Y., Oguma N., 2002, “Characteristic S-N properties of high-carbon-chromium-bearing steel under axial loading in long-life fatigue”, *Fatigue and Fracture of Engineering Materials and Structures*, Vol. 25, 765-773.

[21] Sarpkaya T., 2004, “A critical review of the intrinsic nature of vortex-induced vibrations”, *Journal of Fluids and Structures,* Vol. 19, 389-447.

[22] Sharma A., Oh M.C., Ahn B., 2020, “Recent advances in very high cycle fatigue behavior of metals and alloys - a review”, *Metals,* Vol. 10, 1200.

[23] Shi, Y.M., Gao, F.P., Wang, N., Yin, Z.Y., 2021, “Coupled flow-seepage-elastoplastic modeling for competition mechanism between lateral instability and tunnel erosion of a submarine pipeline”, *Journal of Marine Science and Engineering*, Vol. 9(8), 889.

[24] Shiozawa K., Lu L., Ishihara S., 2001, “S-N curve characteristics and subsurface crack initiation behaviour in ultra-long life fatigue of a high carbon-chromium bearing steel”, *Fatigue & Fracture of Engineering Materials & Structures*, Vol. 24, 781-790.

[25] Song Q., 2021, *Observation of Characteristic and Analysis of Mechanism in Very High Cycle Fatigue Regime of High-Strength Steel*, PhD Thesis, University of Chinese Academy of Sciences, Beijing, China.

[26] Song Q., Sun C., 2020, “Mechanism of crack initiation and early growth of high strength steels in very high cycle fatigue regime”, *Material Science and Engineering A*, Vol. 771, 138648.

[27] Sumer B.M., Jensen H.R., Mao Y., et al., 1988, “Effect of lee-wake on scour below pipelines in current”, *Journal of Waterway Port Coastal and Ocean Engineering,* Vol. 114, 599-614.

[28] Williamson C.H.K., Govardhan R., 2004, “Vortex-induced vibrations”, *Annual Review of Fluid Mechanics,* Vol. 36, 413-455.

[29] Wu X., Ge F., Hong Y., 2012, “A review of recent studies on vortex-induced vibrations of long slender cylinders”, *Journal of Fluids and Structures,* Vol. 28, 292-308.

[30] Yan Y., Zhong S., Chen Z., et al., 2023, “Corrosion fatigue behavior of X65 pipeline steel welded joints prepared by CMT/GMAW baking process”, *Corrosion Science,* Vol. 225, 111568.